Published in final edited form as:
Carbohydr Res. 2014 May 7; 389: 134–140. doi:10.1016/j.carres.2014.02.009.

Conformational changes of 1-4-glucopyranosyl residues of a sulfated C—C linked hexasaccharide

Alessia Coletti[a], **Stefano Elli**[b,*], **Eleonora Macchi**[b], **Patrizia Galzerano**[a], **Leila Zamani**[c], **Marco Guerrini**[b], **Giangiacomo Torri**[b], and **Elena Vismara**[a]

Stefano Elli: elli@ronzoni.it

[a]Department of Chemistry, Materials and Chemical Engineering 'G. Natta', Politecnico di Milano, via L. Mancinelli 7, 20131 Milano, Italy

[b]'G. Ronzoni' Institute for Chemical and Biochemical Research, via G. Colombo 81, 20133 Milano, Italy

[c]Department of Chemistry, Yazd University, PO Box 89195-741, Yazd, Iran

Abstract

This work describes the structure of a fully sulfated maltotriose *alpha–beta* C—C linked dimer, where a central glycosidic bond was substituted by a non natural, hydrolase-resistant C—C bond. Such compound shows anti-metastatic properties being an inhibitor of the heparanase enzymatic activity and of P-selectin-mediated cell–cell interactions. NMR spectroscopy was applied to investigate the structure and conformational properties of this C—C linked hexasaccharide. The presence of sulfate substituents and the internal C—C bond drives the two internal rings in an unusual $^{1}C_{4}$ chair conformation, while the external rings linked by glycosidic bonds retain the typical $^{4}C_{1}$ conformation. The NMR results were confirmed by molecular mechanics calculations using structure corresponding di- and tetrasaccharides as models.

Keywords

Sulfated oligosaccharide-based drugs; Maltotriose; Sulfated C—C oligosaccharides; $^{1}C_{4}$ chair conformation; NOESY spectroscopy; Molecular mechanics

1. Introduction

The natural sulfated polysaccharides heparan sulfate and heparin[1] are involved in many biological processes such as the modulation of heparanase enzymatic activity, inflammation, coagulation, and angiogenesis.[1,2] Due to its anticoagulant activity, heparin has been widely used in clinics. The observation that cancer patients treated with heparin and low molecular weight heparin prolonged their survival, suggested a possible use of heparin as anti-neoplastic drug.[3,4] Further studies demonstrated that heparin plays a role in the prevention of cancer metastasis by inhibition of heparanase,[5,6] a mammalian endo-glycosidase that is

*Corresponding author. Tel.: +39 02 70641627; fax: +39 02 70641634.

up-regulated in essentially all human tumors.[7,8] Unfortunately the strong anticoagulant activity of heparin prevents its use as antimetastatic drug because of bleeding risks. One of the possible approaches to design heparanase inhibiting compounds, is to synthetize mimetics that can interact with the binding site of the enzyme in a similar manner as heparan sulfate, its natural substrate, but cannot be degraded, thus preventing the access of heparan sulfate chains to the catalytic site. Heparan sulfate mimicking molecules having antimetastatic activity but lacking anticoagulant activity, are currently being developed.[9–12] Phosphomannopentaose sulfate (PI-88)[13,14] and maltohexaose sulfate,[13] both considered as functional mimetics of heparan sulfate, show promising antimetastatic, and anti-angiogenic activity in mouse models. In this framework sulfated maltotriose C—C linked dimers (SMTC), which are highly sulfated hexasaccharides obtained by radical dimerization of a maltotriose derivative,[15] have been investigated as antimetastatic agents. The choice of using a hexasaccharide instead of a shorter chain was due to the evidence that a minimum of six D-glucopyranosidic units is requested for their biological activity. In fact, the analogous fully sulfated tetrasaccharides were found to be inactive.[16] It has been shown that depending on the configuration of the central C—C bond linking the two maltotriose moieties through their anomeric carbons, SMTCs can inhibit heparanase.[17] Moreover, the *alpha–beta* stereoisomer was also proved to be an inhibitor of P-selectins, which are vascular cell adhesion molecules responsible for the interaction of tumor cells with blood constituents.[18] Therefore, considering that attenuation of metastasis could be achieved also by inhibition of P-selectins, αβ-SMTC is the most promising compound among the three possible diastereoisomers. This consideration prompted us to deeply investigate the structural features of αβ-SMTC that could be correlated to its biological activity. In this work NMR spectroscopy and molecular mechanics (MM) calculations were used to characterize αβ-SMTC conformational aspects.

2. Results and discussion

2.1. Background and strategy of the study

Semi-synthetic SMTCs were obtained as shown in Scheme 1, by electrochemical reduction over Ag electrode of acetobromomaltotriose,[15] which is a derivative of the natural product maltotriose, as shown in Scheme 1. Being a radical process, the dimerization of acetobromomaltotriose affords the formation of three different acetylated C—C linked hexasaccharide diasteroisomers in statistical ratio (αα:αβ:ββ = 1:2:1). Details of the synthetic process have been previously published.[15,19] After HPLC separation, deacetylation, and sulfation, pure αα, αβ, and bb SMTC diastereoisomers with average sulfation higher than 78%, were obtained and tested as heparanase and P-selectin inhibitors, both in vivo and in vitro experiments. Results obtained showed that the bb compound is not active, while both αα and αβ diastereoisomers showed significant anti-heparanase activity. In addition ab-SMTC was also able to inhibit P-selectins.[18] The difference in biological activity seems related to the configuration of the central C—C bond, which generates the three diastereoisomers, and their allowed conformations. In this work the attention was focused on αβ-SMTC, which is the most biologically active and therefore the most promising compound in this series. The αβ-SMTC structural properties were characterized combining NMR spectroscopy and molecular mechanics approach.

As shown in Scheme 1, each ring of the αβ hexasaccharide is designated by a letter, starting from A from the external ring, and going to F for the opposite ring. This nomenclature was used for αβ-SMTC in a previous work,[15] where the corresponding ^{1}H NMR and ^{13}C NMR signals were assigned. The C—C structural element is defined by few features: (i) the anomeric carbons configuration (α or β); (ii) the torsional angle degree of freedom θ (H^{C1}—C^{C1}—C^{D1}—H^{D1}) (Scheme 1), a parameter defining the oligosaccharide shape (*linear or bent*), that appears to be important in recognition by heparanase; (iii) the glycosidic torsional state conformations inside each maltotriose unit, and (iv) the conformation of glucose rings. This latter point is important for the scope of this study. In fact, while glucopyranosidic residues in oligosaccharides linked by glycosidic bonds are invariably in the $^{4}C_{1}$ chair forms, the conformation of these residues when they are linked directly through their anomeric carbons by a single C—C bond is unknown, and could be $^{4}C_{1}$, $^{1}C_{4}$ or a distorted conformation. These local conformations can be affected by the sulfation degree of each residues, 'driving' their conformation in oligo- or polysaccharides, as observed for glucuronic acid residues in chondroitin sulfates, normally found in $^{4}C_{1}$ form, changing to $^{1}C_{4}$ when chondroitin is fully O-sulfated.[20]

2.2. Strategy: NMR–molecular mechanics on models

2.2.1. NMR characterization—αβ-SMTC and the corresponding nonsulfated precursor αβ-MTC were characterized by NMR spectroscopy, using ^{1}H, TOCSY, HSQC, HMBC, and NOESY techniques, and using a 600 MHz spectrometer. The ^{1}H and ^{13}C chemical shifts together with $^{3}J_{HH}$ coupling constants of nonsulfated hexasaccharides (αβ-MTC) and their sulfated derivatives (αβ-SMTC), were reported by Guerrini et al.[19] and by Vismara et al.[15] respectively. Despite the NOEs due to the vicinal protons, semi-quantitative analysis of the αβ-SMTC NOESY spectrum (Fig. 1), shows *strong* inter-glycosidic NOEs between B1 and C4/C3 and between E1 and D3/D4, confirming the sequence obtained by HMBC spectrum. A deeper analysis of the HMBC spectra of αβ-SMTC allows to discern the wrong assignment of ^{1}H and ^{13}C resonances in Vismara et al.,[15] where the signals of the previously labeled residues 'C' and 'D' were inverted (i.e. resonances of the ring C were labeled D). In Table 1 are reported intra-residue H—H vicinal NOEs for the central C—C linked glycan (residue C and D), together with the corresponding inter proton distances, estimated by modeling after the conformational analysis described in Subsection 2.2.2. On the other hand, the analysis of intra-residue NOEs allowed establishing the chair conformation of the units. While both residue B and E show strong H5–H3, typical for the axial orientation of hydrogen atoms in $^{4}C_{1}$ conformation, a weak or null magnitude of this NOE was observed for residues C and D. These results strongly suggest that the C—C bond, between residues C and D, modifies their conformation from $^{4}C_{1}$ to $^{1}C_{4}$, similarly to what observed for the glucuronic acid residues in fully sulfated chondroitin sulfate.[20] This feature was never observed before for maltose- and maltotriose-like structures, where all residues maintained the $^{4}C_{1}$ conformation. To verify the possibility that the C—C bond can affect the conformation of the involved residues independently from the sterical effect of the sulfate substituents, the NOESY spectrum was measured on the nonsulfated αβ-MTC hexasaccharide, using a 900 MHz NMR spectrometer. The presence of H5-H3 NOE (data not shown) for all glucopyranosidic units indicated that all glucose residues are in the $^{4}C_{1}$ conformation, no matter if the sugar residues are linked directly by C—C or by normal

glycosidic bonds. The change from $^4C_1$ to $^1C_4$ conformation of residue bound through C—C bond is presumably due to a superposition of two effects: the sterical and/or electrostatic repulsion between the bulky sulfate groups, and the C—C link connection involving the two anomeric carbons of αβ-SMTC.

The observed coupling constants ($^3J_{HH}$) help in confirming the conformation of each residue. The small $^3J_{H1–H2}$ and $^3J_{H2–H3}$ coupling constants found for the ring C in αβ-SMTC ($^3J_{HH}$ about 1 Hz) suggest a gauche vicinal conformation, typical for $^1C_4$ chair, thus reinforcing the previous results. On the other hand, the $^3J_{H2–H3}$ and $^3J_{H3–H4}$ of residue E of about 8.8 and 9.3 Hz respectively, confirm the $^4C_1$ conformation of this unit. The θ angle determination for the αβ-SMTC hexasaccharide was based on the $^3J_{H-H}$ (C1–D1) coupling constant (9.2 Hz) that matches with a *trans* conformation. The remaining measurable $^3J_{HH}$(D1–D2) of 1.9 Hz agrees with a *gauche* vicinal conformation that could be found in both α and β $^1C_4$ or α $^4C_1$ chairs. Three NOESY signals across the C—C bond in αβ-SMTC (Fig. 2) reinforce the previous indication on the θ angle conformation: C2-D1, D2-C1, and C1-D1 that are *strong*, *absent*, and *strong* respectively. Table 2 shows how the θ angle for the C—C structure corresponds to value around −160° that qualitatively agrees with a conformation close to the *trans* (180°) and far from the *gauche*(−) (−60°), this latter being forbidden for this molecule, as discussed in the modeling description (Subsection 2.2.2). Noteworthy the C1–D1 NOESY is *strong* even if, for all the tested conformations, the C1–D1 distance still remains fixed around 3 Å. A possible explanation of this finding is the superposition of C1–D1, and D6-D1 NOEs that probably allows to discern a virtual stronger NOE magnitude (Fig. 1). Matching the NOESY constraints across the C—C bond with the $^1C_4$–$^1C_4$ *trans* conformation of αβ-SMC model (see Subsection 2.2.2), and adjusting the θ angle, allowed to assign the a configuration to the D1 carbon of the ring D in the αβ-SMTC, whereas the residue C matches with a β configuration. Although affected by an intense overlap of the signals, a strong C1–C5 NOESY cross-peak was observed for the residue C (Fig. 1), matching with the b $^4C_1$ instead of the hypothesized $^1C_4$ conformation, even if, a strong spin-diffusion effects can be expected. Hence the occurrence of an equilibrium between the two chairs of the residue C could not be excluded.

Analysis of the other inter-residue NOEs of the αβ-SMTC (Fig. 1 insert), allowed to obtain experimental constrains for the geometries of *internal* B–C and E–D and *external* A–B and E–F glycosidic bonds (Scheme 1). The qualitative interpretation of such signals is summarized in Table 3, where the signal intensity and the corresponding estimated distances are reported. The fourth column shows the corresponding H1–H4 and H1–H3 distances for the optimized αβ-SMC tetrasaccharide model as obtained by molecular mechanics conformational search procedure reported in Subsection 2.2.2. The predicted glycosidic torsional angles (ϕ_{ED}/ψ_{ED} = −42/−7° and ϕ_{BC}/ψ_{BC} = −44/−9°, see Fig. 3) based on the αβ-SMC tetrasaccharide analysis well comply with the corresponding NOESY signals measured for αβ-SMTC hexasaccharide related glycosidic junction.

2.2.2. Molecular modeling studies on di- and tetrasaccharides—To evaluate αβ-SMTC structural features using a modeling based procedure, the fully sulfated tetrasaccharide αβ-maltose C—C linked dimer (αβ-SMC), was used as a simplified model. In such structure, where the ring sequence in Figure 3 reproduces the internal structure of

αβ-SMTC of Scheme 1, the two external rings were defined in $^4C_1$ conformation and the internal ones alternatively in $^4C_1$ or $^1C_4$ chairs. These two different conformations were named as $^4C_1$–$^4C_1$ and $^1C_4$–$^1C_4$ respectively, referring only to the two central residues. The basic structure for the corresponding nonsulfated αβ-MC (αβ-maltose C—C linked dimer) in conformation $^4C_1$–$^4C_1$ was taken from the previous study,[19] while the $^1C_4$–$^1C_4$ conformer was obtained by molecular editing of the previous model. All free hydroxyl groups were sulfated and each sulfate group $(-O-SO_3^-)$ was described with a −1 charge, being −14 the total charge for each αβ-SMC molecule.

The conformational analysis of the αβ-SMC can be reduced to the determination of the most probable states for the two glycosidic torsional angles (ϕ_{ED}/ψ_{ED} and ϕ_{BC}/ψ_{BC}) between rings E–D and B–C, and for the central torsional angle θ (see Fig. 3). To achieve this goal using the molecular mechanics approach, the first step consists of the glycosidic bond torsional state analysis applying a combined torsional angle scan/energy minimization procedure, that allows to draw a potential energy map as a function of the ϕ/ψ visited states. This procedure was applied on a further simplified system, the 2,3,6-hexasulfated-maltose in its $^4C_1$–$^1C_4$ and $^4C_1$–$^4C_1$ chairs, that in approximation describes ‘half of αβ-SMC tetrasaccharide in the two chosen limit conformations. Figure 4 shows the potential energy maps obtained using a color code, plotted as a function of the ϕ/ψ torsional angles for the 2,3,6-hexasulfated-maltose disaccharides $^4C_1$–$^1C_4$ (left panel) and $^4C_1$–$^4C_1$ (right panel). From a qualitative point of view few differences can be seen comparing the two plots, meaning that $^1C_4$ or $^4C_1$ chair conformation at the reducing end sugar, does not affect significantly the glycosidic bond potential energy surface of the disaccharides.

The darker blue areas represent torsional angle states with the smaller potential energy for both the tested conformers. Three energy minima were found for $^4C_1$–$^1C_4$ conformer: the first one has a wider area and is located approximately at −50/0° (i.e. in the center of the map), while the remaining two are narrower and located at −25/−175° and −50/150°. For the $^4C_1$–$^4C_1$ conformer the corresponding minima were located respectively −50/50°, 0/−175°, and −50/175°. For both conformers only the first cited energy minimum has significant torsional states, while the second and the third ones correspond to conformers where the H1–H4 or H1–H3 distances across the glycosidic bond are too long (>3.0 Å) to be supported by the qualitative interpretation of the NOESY spectrum of αβSMTC hexasaccharide, as seen in the NMR section (Subsection 2.2.1). Analogously the ϕ/ψ scan was applied to the two corresponding nonsulfated maltoses, having (as before) the reducing end residue in $^1C_4$ and $^4C_1$ conformations. Even in that case, the two potential energy maps report few qualitative differences, and determine three energy minima (maps not reported). As discussed before, only one minimum gives a meaningful glycosidic torsional state, approximately located at −50/0°.

The glycosidic ϕ/ψ torsional angle states estimated from these potential energy maps, were used to guess the initial conformation of the αβSMC tetrasaccharide in $^1C_4$–$^1C_4$ and $^4C_1$–$^4C_1$ conformation, together with the corresponding nonsulfated molecules. After that, scan/potential energy minimization was applied on the central θ torsional angle of each structure (see Section 4 for setting details). It is important to specify that for each θ value explored, the energy minimization stops when the gradient threshold condition is reached,

meaning that the tested geometry corresponds to an energy minimum for the remaining degrees of freedom of the molecule. Such approach gives an idea about the possible conformations around the central C—C anomeric carbon linkage of both tetra- and hexasaccharides. Figure 5 represents the potential energy profiles obtained for the four tetrasaccharide models: αβ-SMC (upper curves) and αβ-MC (lower curves), where in both cases red and black lines with filled dots correspond to $^{1}C_{4}$–$^{1}C_{4}$ and $^{4}C_{1}$–$^{4}C_{1}$ chairs respectively. Qualitatively comparing the potential energy/θ profiles in Figure 5 it is evident how the αβ-MC curves show a smoother shape compared to αβ-SMC ones. More accurate αβ-MC curves show three clearly defined minima and maxima, while αβ-SMC profiles show only two physically meaning minima connected by one maximum for the red curve and two maxima for the black curve, being respectively $^{1}C_{4}$–$^{1}C_{4}$ and $^{4}C_{1}$–$^{4}C_{1}$ conformers. In fact, for the αβ-SMC in $^{1}C_{4}$–$^{1}C_{4}$ conformation (red upper curve in Fig. 5), the θ angle region (approximately between [−120, 30°]) corresponds to several sterically forbidden states, represented by at least two discontinuities of $E(\theta)$, located approximately between [−100, −90°] and [−11, 9°].

The increase of roughness in the potential energy profile curves going from nonsulfated to sulfated tetrasaccharides is correlated to the increase of sterical hindrance around the C—C linked region due to bulky sulfate groups, that reduce the number of physically available states for the torsional θ angle. In αβ-SMC the region of sterically forbidden conformations is wider compared to the two located discontinuities and it cannot be easily identified by very high energy values, because the potential energy function does not describe accurately the molecule behavior when some of its atoms are located at very small distances, that is comparable to their van der Waals radius. The properties of the significant conformations, corresponding to minima points of the energy profile in Figure 5, are reported in Tables 4 and 5 for the fully sulfated αβ-SMC and not sulfated αβ-MC in the order.

The MM description of the fully sulfated C—C linked dimer αβ-SMC in the $^{1}C_{4}$–$^{1}C_{4}$ conformation has an absolute minimum at 180° (*trans*) and an additional conformation at 80° (*gauche* (+)). Differently the $^{4}C_{1}$–$^{4}C_{1}$ conformation has an absolute energy minimum at −100° (*gauche* (−)) and an additional minimum at 170° (*trans*). Interestingly, the allowed minima for θ in $^{1}C_{4}$–$^{1}C_{4}$ conformation of αβ-SMC have a smaller energy content compared to what is found for $^{4}C_{1}$–$^{4}C_{1}$, (see Fig. 5 and Table 4). This analysis predicts for αβ-SMC a preferred $^{1}C_{4}$–$^{1}C_{4}$ *trans* conformation (θ = 180°), which is respectively 3.7 and 5.8 Kcal mol^{-1} lower in potential energy scale compared to the $^{1}C_{4}$–$^{1}C_{4}$ *gauche* (+) (θ = 80°) and $^{4}C_{1}$–$^{4}C_{1}$ *gauche* (−) (θ = −100°) conformations.

The conformational refining of αβ-SMC was done setting θ = 180° and the two glycosidic bonds ϕ;$_{ED}$/ψ;$_{ED}$ = ϕ;$_{BC}$/ψ;$_{BC}$ = −50/0° in accord to the potential energy maps in Figure 4, a final energy minimization does not change significantly the parameters θ =−177°, ϕ;$_{ED}$/ψ;$_{ED}$ = −42/−7° and ϕ_{BC}/ψ;$_{BC}$ = −44/−9°, meaning that the conformation of the tetrasaccharide could be estimated starting from suitably chosen disaccharides as models. Using the same idea the C—C linked tetrasaccharide, reproduces at first level of approximation, the longer hexasaccharide. A graphical representation of the αβ-SMTC hexasaccharide predicted conformation is given in the graphical abstract of this paper, where the impact given by the central ring conformations $^{1}C_{4}$–$^{1}C_{4}$ or $^{4}C_{1}$–$^{4}C_{1}$ on the whole

structure, can be visualized. These results match qualitatively with ^{1}H NOESY spectra and $^{3}J_{HH}$ coupling interpretation of αβ-SMTC, as seen previously in NMR section (Subsection 2.2.1).

The molecular mechanics conformational description of the $^{1}C_{4}$–$^{1}C_{4}$ and $^{4}C_{1}$–$^{4}C_{1}$ nonsulfated αβ-MC was carried out in order to understand if the conformational change from $^{4}C_{1}$ to $^{1}C_{4}$ chair predicted for the C—C linked residues of αβ-SMTC is related to a combination of the sterical hindrance effect of the sulfate groups and the C—C linked connectivity involving the two anomeric carbons. From Figure 5 (lower curves) and Table 5, αβMC in $^{1}C_{4}$–$^{1}C_{4}$ conformation has an absolute minimum at $\theta = 180°$ (*trans*) conformation lower in energy of about 1 Kcal mol^{-1} compared to the two *gauche* (+) and *gauche* (−) located at 60 and −60° respectively, showing approximately the same energy. Interestingly the MC conformer $^{4}C_{1}$–$^{4}C_{1}$ shows a lower amount of energy for each value of θ, compared to the $^{1}C_{4}$–$^{1}C_{4}$ profile. In fact for αβ-MC the $^{4}C_{1}$–$^{4}C_{1}$ conformation has three minima located at 180°, −81°, and 60° (Fig. 5 lower black curve and Table 5 right) corresponding to a *trans* and two *gauche* conformations. Finally the MM description applied on αβ-MC predicts a preferred $^{4}C_{1}$–$^{4}C_{1}$ *trans* ($\theta = 180°$), followed by a $^{4}C_{1}$–$^{4}C_{1}$ *gauche* (−) ($\theta = -81°$), and by the opposite *gauche* (+) ($\theta = 60°$), last two being higher in energy respectively 1.5 Kcal mol^{-1} and 4.7 Kcal mol^{-1} compared to the *trans* form. The energy difference between the *trans* and *gauche* (−) states is then comparable to the average system thermal energy at $T = 300$ K (about 0.3 Kcalmol^{-1}), allowing both states to be populated, in fact the Boltzmann factor between these two states predicts a distribution of 90% and 10% for the *trans* and *gauche* (−). The opposite ratio between *trans* and *gauche* (−) states for θ degree of freedom, is supported by the experimental data shown by Guerrini et al.[19] where $^{3}J_{HH}$(C1–D1) measured on maltose C—C linked dimer is 2.5 Hz. In fact this value is consistent with a mixture between a more populated *gauche* (−) and a less populated *trans* conformations, corresponding to coupling constant values of 0.8 Hz and 9.8 Hz respectively, as estimated by ‘Maestro9.8 ′ graphical interface.

The molecular mechanics analysis of αβ-SMC shows also how the $^{1}C_{4}$–$^{1}C_{4}$ conformations allows a smaller sterical hindrance compared to the $^{4}C_{1}$–$^{4}C_{1}$, this results become understandable decomposing the potential energy difference between the two tested conformation ($^{1}C_{4}$–$^{1}C_{4}$ and $^{4}C_{1}$–$^{4}C_{1}$) in the internal degree of freedom terms: *connectivity energy term* (*stretching* and *bending*), *torsion*, *van der Waals*, and *electrostatic*, as reported in the last row of Table 6. Table 6 shows how the connectivity term (stretching and bending) of the potential energy, has the greater differences between the two conformations, while differently from what expected, the *electrostatic* contribution is significantly less important, at least in this static description. This result shows how the sterical hindrance plays a major role in driving the conformation of the C—C linked rings, from $^{4}C_{1}$–$^{4}C_{1}$ to the favorite $^{1}C_{4}$–$^{1}C_{4}$.

3. Conclusions

In this study the conformational characterization of the fully sulfated maltotriose C—C linked dimer αβ-SMTC is presented, based on NMR measurements and on molecular mechanics conformational search on analogous di- and tetrasaccharides. A deeper structural

investigation for this αβ-SMTC oligosaccharide is required, due to its unusual chemical structure, and for a promising inhibitory activity of heparanase and P-selectins. NOE spectroscopy and coupling constant $^{3}J_{HH}$ investigation of αβ-SMTC suggested that both the C—C ring connectivity and the presence of sulfate groups determine the preferred $^{1}C_{4}$ chair conformation of the two directly C—C linked residues; on the other hand, external residues not involved in the C—C bond linkage maintain the $^{4}C_{1}$ conformation commonly found for glucopyranosidic residues in natural oligosaccharides where extra-ring connectivities are allowed through glycosidic bonds. Potential energy analysis and coupling constant $^{3}J_{HH}$ measurements predict also for αβ-SMTC a *trans* conformation for the central torsional angle (θ), in agreement with a qualitative interpretation of the NOESY spectrum, while the *gauche* (−) appears to be preferred for the analogous nonsulfated structure, in agreement with the corresponding $^{3}J_{HH}$ constants published previously by Guerrini et al. [19] and partially with the modeling description presented in this paper. The molecular mechanics approach suggested also the sterical hindrance as the main parameter affecting the preferred chair conformation of C—C linked residues, while electrostatic repulsions among sulfate groups appear to play a minor role. Extending this study to the acetylated precursor of the αβ-SMTC, where the acetyl group substituents do not have an electrostatic charge, but still maintain a significant sterical hindrance, should allow a better understanding of the role of these driving forces on the chair ring conformational equilibrium for this restricted class of oligosaccharides.

4. Experimental section

4.1. NMR experiment and sample preparation

About 15 mg of αβ-SMTC was dissolved in 0.6 mL of deuterium oxide. NMR spectra of αβ-SMTC were measured at 303 K using a 600 MHz Bruker Avance spectrometer equipped with a high sensitivity 5 mm TCI cryoprobe. 7.5 mg of αβ-MTC was dissolved in 0.6 mL of deuterium oxide, then the sample was characterized using a 900 MHz Bruker Avance, equipped with a high sensitivity 5 mm TCI cryoprobe. Two-dimensional (2D) NMR experiments were conducted using edited HSQC, COSY, HMBC, TOCSY, and NOESY (using different mixing times 300 and 500 ms), recorded for quadrature detection in the indirect dimension and acquired using 8-128 scans per series of 1024 × 320 data points, with zero filling in F1 (4096) prior to Fourier transformation. HSQC experiments were recorded with a spectral width of 12 ppm in F2 and 70 ppm in F1 with a relaxation delay of 2 s. NOESY experiments were recorded using a spectral width of 3.9 ppm in both the dimensions and with a relaxation delay of 7 s. COSY and TOCSY experiments were recorded using a spectral width of 3.9 ppm both in F1 and F2, with a relaxation delay of 2 s. HMBC experiments were recorded using a spectral width of 7 ppm in F2 and 90 ppm in F1, with a relaxation delay of 2 s and 128 scans. The temperature of the experiments was set at 303 K.

4.2. Molecular mechanics conformational characterization

The software used for molecular editing and computational description is ‘Maestro-9.0/ Macromodel-9.8′. The Force Field used is the Amber* including Homans parameter for carbohydrates, where the atomtype assigned for each described atom belongs to the

Macromodel atomtype set. Non bonded interactions are treated using the standard cut-off technique, setting it to: 12.0, 7.0, and 4.0 Å for electrostatic, van der Waals, and hydrogen bond interactions respectively. The water solvent environment around the molecule is implicitly described by a continuum with a fixed dielectric constant value 80.0. The energy minimization procedure (batchmin) applied several times during the conformational search (before each torsional angle scan, and for every applied torsional angle step), uses 5000 minimization steps, or an energy gradient threshold of 10^{-3} KJ mol^{-1} $Å^{-1}$. The energy minimization algorithm applied is the default method (PRGC) implemented in 'Macromodel-9.8′ software. The torsional angle scan/energy minimization procedure applied on the previously mentioned models of: 2,3,6-hexasulfated-maltose disaccharides, is done changing glycosidic ϕ/ψ angles one at a time within a range of [−180, 180] degree using an angle step of 15°, after every torsional angle increment an energy minimization procedure is applied using 5000 steps or until the energy gradient reaches the absolute value 10^{-3} KJ mol^{-1} $Å^{-1}$. The torsional angle scan/energy minimization applied on the θ degree of freedom, was done using an interval [−180, 180°] with an angle increment of 10°, while the potential energy minimization applied to every angle increment includes at least 5000 steps or a gradient threshold of 10^{-3} KJ mol^{-1} $Å^{-1}$.

Acknowledgments

This work was co-supported by the US National Institute of Health (grant number R01-CA138535), and by 'G. Ronzoni' Foundation for Chemical and Biochemical Research, Milano (Italy).

We are grateful for access to the NMR spectrometer (900 MHz) at the Utrecht NMR Facility and the assistance of Dr. Hans Wienk.

We are thankful to Dr. B. Casu and Dr. A. M. Naggi for useful discussions.

References

1. Garg, HG.; Linhardt, RJ.; Hales, CA. Chemistry and Biology of Heparin and Heparan Sulfate. Elsevier; New York, NY, USA: 2005.
2. Bishop JR, Schuksz M, Esko JD. Nature. 2007; 446:1030–1037. [PubMed: 17460664]
3. Zacharski LR, Ornstein DL, Mamourian AC. Semin Thromb Hemost. 2000; 26:69–77. [PubMed: 11011810]
4. Smorenburg SM, Hettiarachchi RJ, Vink R. Thromb Haemost. 1999; 82:1600–1604. [PubMed: 10613641]
5. Hostettler N, Naggi A, Torri G, Casu B, Vlodavsky I, Borsig L. FASEB J. 2007; 21:3562–3572. [PubMed: 17557930]
6. Lerner I, Baraz L, Pikarsky E, Meirovitz A, Edovitsky E, Peretz T, Vlodavsky I, Elkin M. Clin Cancer Res. 2008; 14:668–676. [PubMed: 18212251]
7. Barash U, Cohen-Kaplan V, Dowek I, Sanderson RD, Ilan N, Vlodavsky I. FEBS J. 2010; 277:3890–3903. [PubMed: 20840586]
8. Levy-Adam F, Ilan N, Vlodavsky I. Semin Cancer Biol. 2010; 20:153–160. [PubMed: 20619346]
9. Coombe RD, Kett WC. Heparin Mimetics. Heparin – A Century of Progresses Handbook of Experimental Pharmacology. 2012; 207:361–383.
10. Basche M, Gustafson DL, Holden SN, O' Bryant CL, Gore L, Witta S. Clin Cancer Res. 2006; 12:5471–5480. [PubMed: 17000682]
11. Ferro V, Liu L, Johnstone KD, Wimmer N, Karoli T, Handley P. J Med Chem. 2012; 55:3804–3813. [PubMed: 22458531]

12. Ritchie JP, Ramanil VC, Ren Y, Naggi AM, Torri G, Casu B, Penco S, Pisano C, Carminati P, Tortoreto M, Zunino F, Vlodavsky I, Sanderson RD, Yang Y. Clin Cancer Res. 2011; 17:1382–1393. [PubMed: 21257720]
13. Parish CR, Freeman C, Brown KJ, Francis DJ, Cowden WB. Cancer Res. 1999; 59:3433–3441. [PubMed: 10416607]
14. Joyce JA, Freeman C, Meyer-Morse N, Parish RC, Hanahan D. Oncogene. 2005; 24:4037–4051. [PubMed: 15806157]
15. Vismara E, Coletti A, Valerio A, Naggi A, Urso E, Torri G. Molecules. 2012; 17:9912–9930. [PubMed: 22902885]
16. Vismara E. unpublished results.
17. Borsig L, Vlodavsky I, Ishai-Michaeli R, Torri G, Vismara E. Neoplasia. 2011; 13:445–452. [PubMed: 21532885]
18. Läubli H, Borsig L. Cancer Microenviron. 2010; 3:97–105. [PubMed: 21209777]
19. Guerrini M, Guglieri S, Santarsiero R, Vismara E. Tetrahedron: Asymmetry. 2005; 16:243–253.
20. Maruyama T, Toida T, Imanari T, Yu G, Linhardt RJ. Carbohydr Res. 1998; 306:35–43. [PubMed: 9691438]

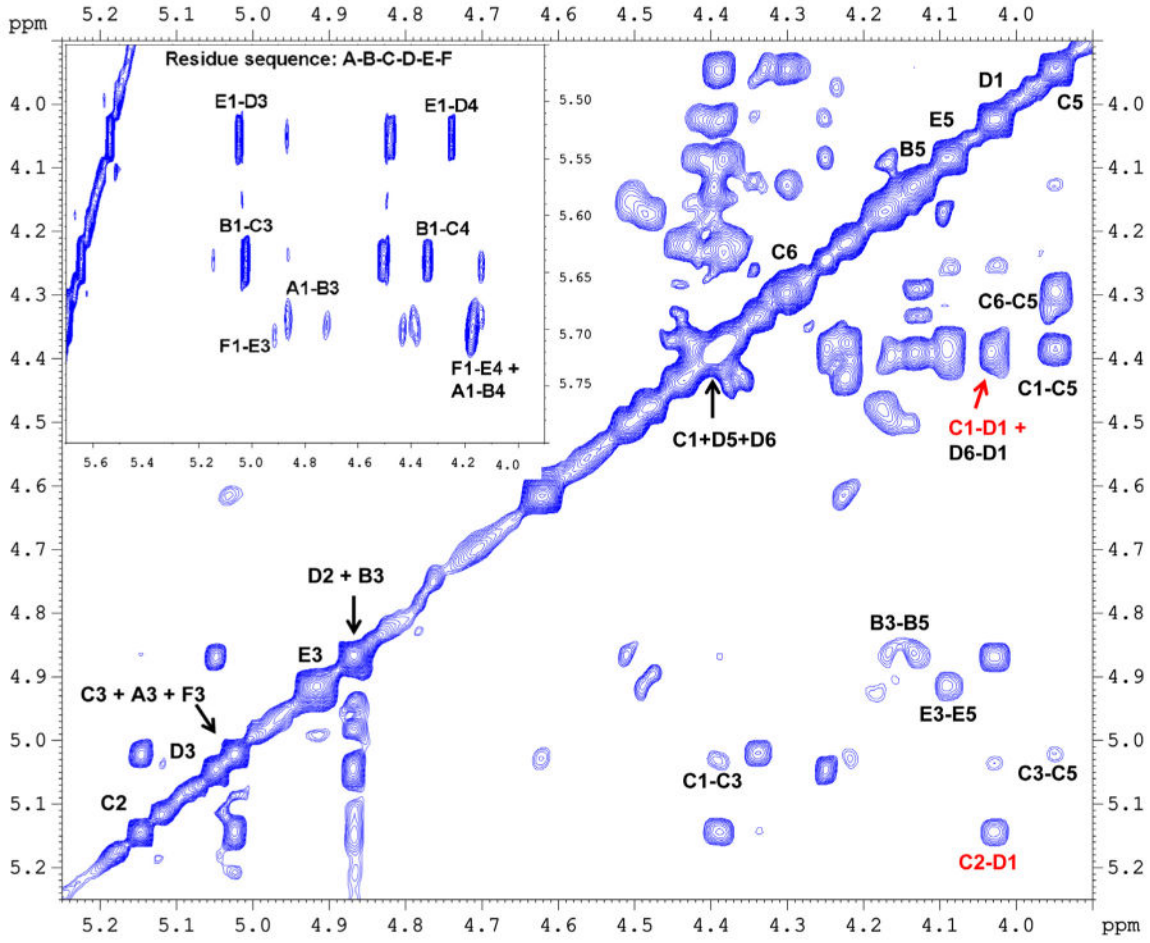

Figure 1.

^{1}H NOESY spectrum of αβ-SMTC recorded at 600 MHz. The ^{1}H signals in accord with the HSQC spectrum are indicated by two types of label: a letter indicating the glycan ring of the sequence A–B–C–D–E–F, followed by a number corresponding to the position inside each residue. Red labels underline NOESY across the C—C bond. The insert is the enlargement of the NOESY spectrum from 5.70 to 3.90 ppm in F2 and from 5.80 to 5.45 ppm in F1, highlighting the H1–H4 and H1–H3 interglycosidic signals for the residues external to the C—C link.

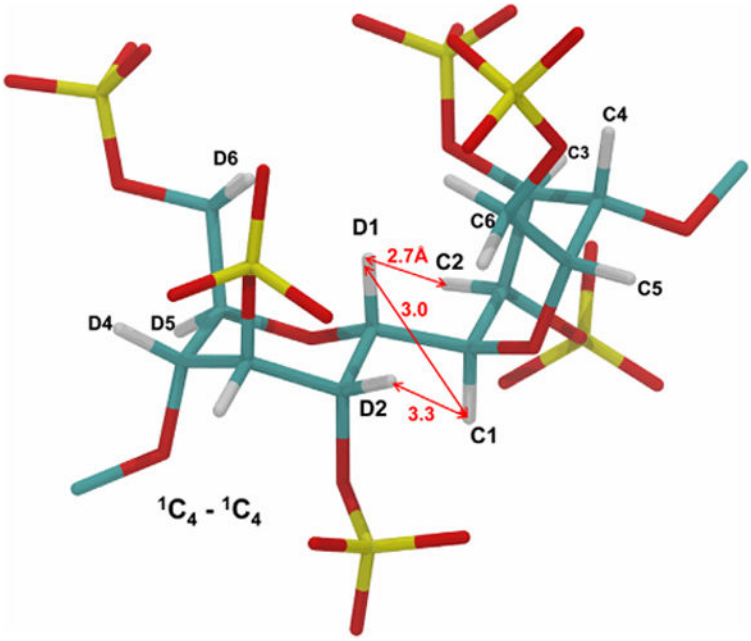

Figure 2.

Suggested conformation of the C—C linked residues (rings C and D) belonging to αβ-SMC in agreement with data reported in Figure 5. The picture shows the arrangement of central residues in $^1C_4$ conformation and a torsional angle $\theta = 180°$ as obtained by molecular mechanics analysis and interpretation of the NOESY spectrum reported in Subsections 2.2.1 and 2.2.2. Arrows show protons correlated by NOESY signals as reported in Table 2.

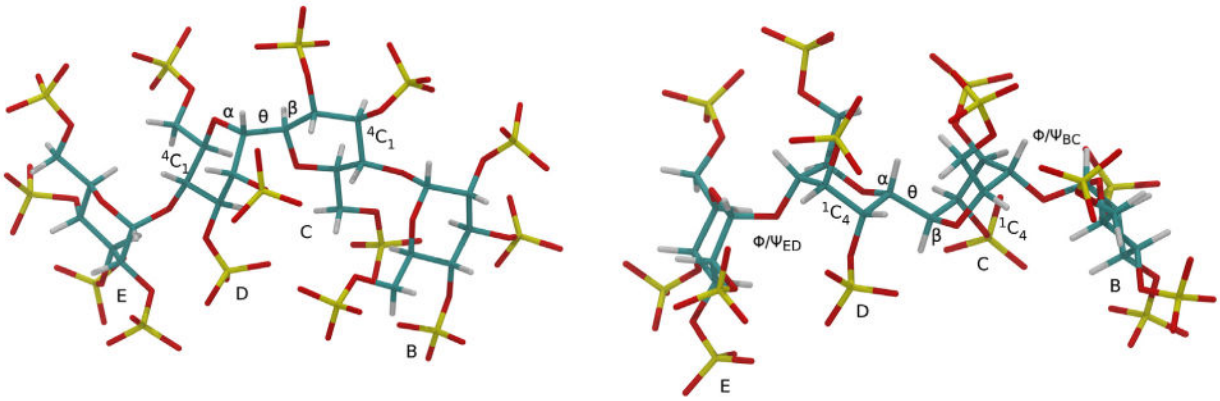

Figure 3.

Two possible conformations of the sulfated αβmaltose CAC linked dimer (αβSMC) considered in this study as a simplified model of the αβ-SMTC. Left: $^4C_1$–$^4C_1$, where the four rings E, D, C, and B show the $^4C_1$ chair conformation. Right: $^1C_4$–$^1C_4$ where the two central rings C and D are reported in $^1C_4$ chairs, while the external rings E and B are represented in the $^4C_1$ conformation as usual for sulfated glucose units.

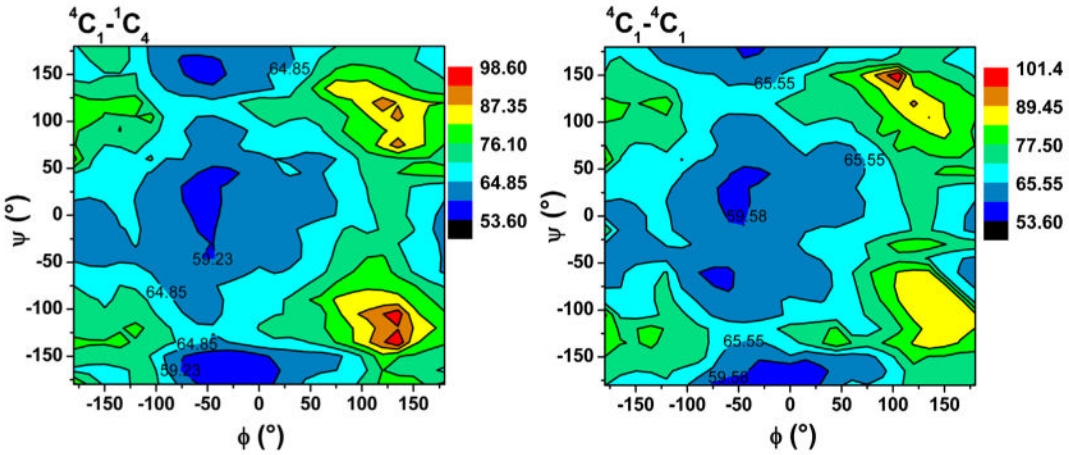

Figure 4.

Potential energy maps for 2,3,6-hexasulfated maltose having the reducing residues in $^4C_1$–$^1C_4$ (left panel) and $^4C_1$–$^4C_1$ (right panel) conformations, obtained by the torsional angle scan/energy minimization procedure. The energy scale is in Kcal mol^{-1}, while angles are expressed in degrees.

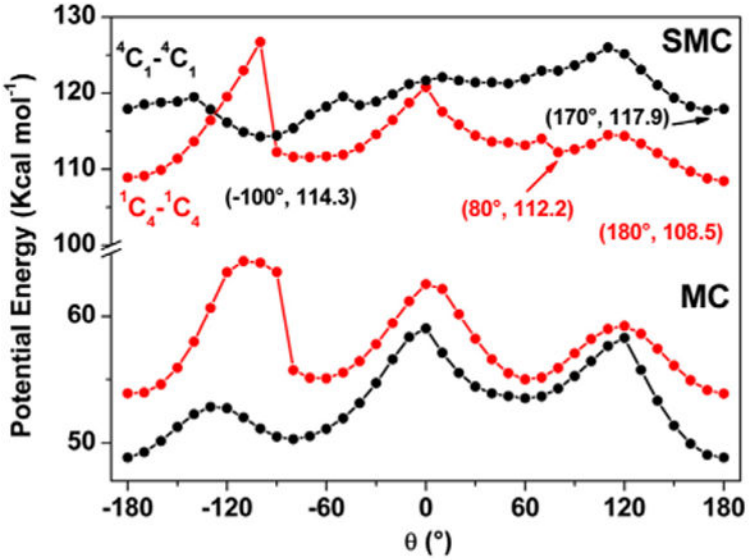

Figure 5.

Potential energy profile (Kcal mol^{-1}) as a function of the θ torsional angle (H^{C1}–C^{C1}–C^{D1}–H^{D1}) for the sulfated-αβ-maltose C—C linked dimer (αβ-SMC, upper curves) and αβmaltose C—C linked dimer (αβ-MC, lower curves). For both αβ-SMC and αβ-MC models the red and black lines with filled dots correspond to the conformers with the C—C linked residues in $^1C_4$–$^1C_4$ and $^4C_1$–$^4C_1$ chair respectively. θ angle and potential energy values of interesting minima are reported in round brackets.

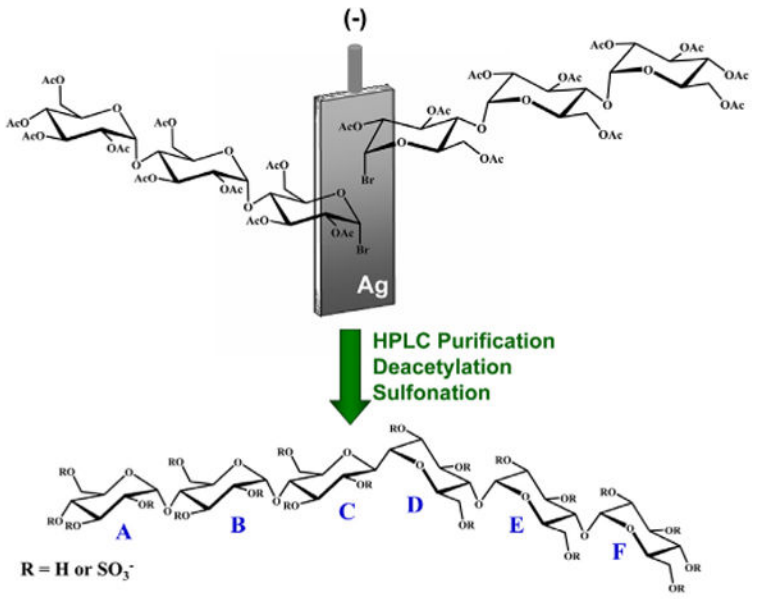

Scheme 1.

Schematization of the synthetic procedure for αβ-SMTC. Letters A, B, C, D, E, and F indicate each hexasaccharide glucose ring.

Table 1

H–H NOESY signals of αβ-SMTC showing residues C and D measured at mixing time of 300 ms

Intra residue conformation			
NOESY	**Intensity**	**Distance (Å) $^{1}C_{4}$**	**Distance (Å) $^{4}C_{1}$**
C1–C2	*Strong*	**2.5**	3.0
C2–C3	*Strong*	**2.5**	3.0
C3–C4	*Strong*	**2.6**	3.0
C1–C3	*Weak*	**4.2**	2.9
C3–C5	*Weak*	**4.2**	2.3
C1–C5	*Strong*	**4.0**	**2.5**
D1–D2	*Strong*	**2.4**	**2.3**
D2–D3	*Strong*	**2.6**	3.0
D3–D4	*Strong*	**2.5**	3.0
D3–D5	*Absent*	**4.2**	2.3
D6–D1	*Strong**	**2.5**–**3.0**	>4.0

The reported distances were obtained from the modeling of αβ-SMC in both forms: $^{1}C_{4}$–$^{1}C_{4}$ *trans* and $^{4}C_{1}$–$^{4}C_{1}$ *gauche*, following the conformational search in Subsection 2.2.2. The bold face types highlight qualitative agreement between NOESY measured intensities and H–H distances obtained at the end of the conformational search. The (*) underlines the strong H–H NOESY of the D6–D1 superposed to D1–C1 signal.

Table 2

Qualitative NOESY intensities between selected protons across the C—C bond of αβ-SMTC

C—C interresidue conformation			
NOESY	**Intensity**	**Distance**	**$\theta(H^{C1}–C^{C1}–C^{D1}–H^{D1})$**
C2–D1	*strong*	**2.7**	**−160.0**
		2.8	−170.0
		2.9	180.0
D2–C1	*absent*	**3.3**	**−160.0**
		3.2	−170.0
		3.1	180.0
C1–D1	*strong*	3.0	−160.0
		3.0	−170.0
		3.0	180.0

The inter proton distances and the corresponding torsional angle $H^{C1}–C^{C1}–C^{D1}–H^{D1}$ values are obtained starting from the simplified model αβ-SMC after the conformational search in Subsection 2.2.2, adjusting the θ angle around the *trans* conformation, until a qualitative match between NOESY intensities and distances becomes possible (see Subsection 2.2.1). The θ angle values that better agree with the NOESY are underlined in bold.

Table 3

Inter-glycosidic H1–H4 and/or H1–H3 NOESY signal intensities and qualitative estimation of the corresponding inter-proton distances for the αβ-SMTC

Interglycosidic conformation			
NOESY	**Intensity**	**Distance**	**MM Conformation**
B1–C4	*strong*	2.4–2.7	3.0
B1–C3	*strong*	2.4–2.7	2.2
E1–D4	*strong*	2.4–2.7	2.3
E1–D3	*strong*	2.4–2.7	2.8
F1–E4 and A1–B4	*Strong*	2.4–2.7	
F1–E3 and A1–B3	*Weak*	>3.0	

The fourth column reports the corresponding measured inter-glycosidic H–H distances from the αβ-SMC model obtained by molecular mechanics analysis as reported in Subsection 2.2.2.

Table 4

θ Torsional angle conformations for αβ-SMC, corresponding to minima of the potential energy profile reported in Figure 5.

αβ-SMC $^1C_4$–$^1C_4$			αβ-SMC $^4C_1$–$^4C_1$		
θ	**Energy (Kcal mol^{-1})**	**Conformation**	***θ***	**Energy (Kcal mol^{-1})**	**Conformation**
[−120 ÷ 30]	Forbidden	–	**−100**	**114.3**	***gauche***(−)
80	112.2	*gauche*(+)			
180	**108.5**	***trans***	170	117.9	*trans*

θ Angle values corresponding to an absolute minimum of the profile are highlighted in bold face.

Table 5

θ Torsional angle conformations for αβ-MC, corresponding to minima of the potential energy profile reported in Figure 5

αβ-MC $^1C_4$–$^1C_4$			αβ-MC $^4C_1$–$^4C_1$		
θ	**Energy (Kcal mol $^{-1}$)**	**Conformation**	**θ**	**Energy (Kcal mol $^{-1}$)**	**Conformation**
−60	55.1	*gauche*(−)	−81	50.4	*gauche*(−)
60	55.0	gauche(+)	60	53.6	*gauche*(+)
180	**53.9**	***trans***	**180**	**48.9**	***trans***

θ Angle values corresponding to an absolute minimum of the profiles are highlighted in bold face.

Table 6

Potential energy decomposition (Kcal mol^{-1}) in different terms: stretching, bending, torsion, van der Waals, and electrostatic for $^{1}C_{4}$–$^{1}C_{4}$ *trans* and $^{4}C_{1}$–$^{4}C_{1}$ *gauche*(−) of αβ-SMC

αβ-SMC	*Stretching + Bending*	*Torsion*	*VdW*	*Electrostatic*
$^{1}C_{4}$–$^{1}C_{4}$	37.0	56.9	−14.2	28.6
$^{4}C_{1}$–$^{4}C_{1}$	41.4	57.4	−12.3	27.8
Difference ($^{1}C_{4}$–$^{4}C_{1}$)	**−4.4**	−0.5	−1.9	0.8

The fourth row includes the differences between the second and the third ones. The sum of stretching and bending terms represents the contribution of the connectivity on the potential energy.